Self-Assembly of Latex Particles into Proton-Conductive Membranes

Jun Gao,[†] Yunsong Yang,[‡] David Lee,[†] Steven Holdcroft,[‡,§] and Barbara J. Frisken*,[†]

Department of Physics and Department of Chemistry, Simon Fraser University, 8888 University Drive, Burnaby, BC V5A 1S6, Canada, and Institute for Fuel Cell Innovation, National Research Council of Canada, 4250 Westbrook Mall, Vancouver, BC V6T 1W5, Canada

Received March 2, 2006; Revised Manuscript Received July 12, 2006

ABSTRACT: We present results from our investigation of the concept and practice of using surface-charged latex nanoparticles as building blocks for conductive membranes. Nanoparticles were synthesized in water by free-radical copolymerization of two hydrophobic monomers, butyl acrylate (BA) and methyl methacrylate (MMA), a cross-linker, *N,N*′-methylenebis(acrylamide) (BIS), and a charged monomer, sulfonate styrene sodium salt (NaSS). The resultant nanospheres were characterized with static and dynamic laser light scattering. Thin films were cast from dispersions of particles, followed by incubation at ∼110 °C to yield free-standing membranes. Conductivity, water uptake, and ion exchange capacity were measured. The membranes possess higher conductivities than both amorphous films cast from sulfonated poly(BA−MMA−styrene) ionomers and poly(BA−BIS−MMA−NaSS) gel films. TEM images provide visual evidence of particle and film structure and suggest the existence of continuous hydrophilic channels formed naturally through close-packing of surface-charged nanospheres. Neutron scattering confirms the particulate structure of the membranes.

Introduction

Interest in the properties of proton-conductive membranes, especially for application in polymer electrolyte membrane fuel cells, has increased in the past decade.[1−7] While chemical stability and mechanical strength are necessary requirements, good proton conductivity is also used to identify promising candidates for fuel cell membranes. A suitable membrane must possess sufficient acidic groups to allow a continuous pathway for proton conduction and sufficient hydrophobic chain segments to constrain the swelling of the membrane and to endow it with adequate mechanical strength. Balance between these two aspects can be difficult to achieve because of the incompatibility of the charged and hydrophobic moieties.

Two different strategies have been followed to achieve this balance in proton-conductive membranes. One is to synthesize polymers containing both hydrophobic and ionic groups followed by membrane formation, with perfluoro sulfonated ionomers and in particular Nafion being the prototypical examples.[8] Other examples include polyimides,[9] polybenzimidazoles,[10] poly(ether ether ketones),[11] and polysulfones.[12] The other strategy is to prepare membrane composites, from both proton-conducting and membrane-forming components, including blends,[13] complexes,[14] organic/inorganic composites,[15] and proton-conductive materials in gel hybrids[16] or porous matrixes.[17]

No matter which strategy is chosen, the final morphology of the membrane is crucial to its proton conductivity. It is generally recognized that the final, hydrated membrane should have a bicontinuous nanostructure.[7] For example, it is generally believed that the positive attributes of Nafion as a fuel cell membrane are related to extensive nanoscale phase separation within the membrane.[8,18] An added complication is that the final morphology can depend on how the membrane is formed as well as its thermal history. For example, the ionic conductivity found upon dissolving and recasting commercial Nafion membranes can be 4 orders of magnitude lower than that of the membrane as received.[19]

Recently, we proposed a simple model system designed to facilitate study of the link between structure and conductivity.[20] Our system is based on the use of surface-charged nanospheres as building blocks for proton conductive membranes. Conducting membranes are obtained by casting a concentrated water dispersion of these particles, followed by incubation of partially dried films at elevated temperatures.

In this paper, we provide further details of this process and elaborate on evidence for enhanced conductivity. The nanospheres have lightly cross-linked, hydrophobic cores and proton-conducting surfaces. Four components including two neutral monomers, butyl acrylate (BA) and methyl methacrylate (MMA), a cross-linker *N,N*′-methylenebis(acrylamide) (BIS), and a charged monomer sulfonate styrene sodium salt (NaSS) are used for nanoparticle syntheses using the standard techniques of free-radical emulsion copolymerization in water. The low-T_g component BA was chosen to ensure a low enough T_g of the final particles to obtain a suitable minimum film temperature (MFT).[21,22] The BIS concentration used was low enough to allow for interparticle chain tangling to occur upon annealing but high enough to ensure the persistence of particle structure.[22] The conductivity of the membranes formed by annealing the cast films is compared to that of two classes of membranes of similar charge content but less structural order: membranes cast from randomly copolymerized ionomer chains and thin films formed from polymer gels.

Experimental Section

Particle Synthesis. MMA (99%), BA (99%), BIS, NaSS·xH$_2$O (containing 10 wt % water), and potassium persulfate (KPS, reagent grade) were obtained from Aldrich-Sigma and used as received. A Milli-Q Plus water purification system (Millipore, Bedford, MA) was used to provide purified water for these experiments; particulate matter was removed with a final 0.2 μm filter.

Water-soluble monomers, BIS (400 mg) and NaSS (0−1.44 g), were first dissolved in water (192 mL) and then heated in a flask under a nitrogen atmosphere to an incubation temperature of 70

[†] Department of Physics, Simon Fraser University.
[‡] Department of Chemistry, Simon Fraser University.
[§] National Research Council of Canada.
* To whom correspondence should be addressed.

°C. The reaction was initiated by adding ∼2 mL of KPS solution containing a total of 80 mg of KPS. Non-water-soluble monomers MMA (2.16 mL) and BA (2.16 mL), for a total mass of 4.0 g, were added to the flask immediately before the KPS solution.

Laser Light Scattering. The size, molecular weight, and solid density of the particles were characterized by laser light scattering. The apparatus used for these measurements was an ALV-5000 spectrometer/goniometer equipped with a digital correlator and a helium−neon laser. Light scattering measurements were made on dilute dispersions with concentrations of about 0.1 mg/mL.

We used static light scattering (SLS) to measure the weight-average molar mass M_w and the z-average root-mean-square radius of gyration R_g of the particles. For small particles, we used a standard Zimm plot analysis to find M_w and R_g from the Rayleigh ratio $R_{vv}(q)$ determined from the time-averaged scattered intensity[23]

$$\frac{Kc}{R_{vv}(q)} \cong \frac{1}{M_w}\left(1 + \frac{1}{3}R_g^2 q^2\right) + 2A_2 c \tag{1}$$

where $K = 4\pi^2 n^2 (dn/dc)^2/(N_A\lambda_0^4)$, $q = (4\pi n/\lambda_0)\sin(\theta/2)$ is the scattering wave vector, and A_2 is the second virial coefficient, with N_A, n, c, λ_0, and θ being Avogadro's constant, refractive index of the solvent, concentration (g/mL), wavelength of light in a vacuum, and scattering angle, respectively. We chose a dn/dc value of 0.15 mL/g for all calculations of molar masses based on a mass average of dn/dc values of 0.15, 0.14, and 0.15 for PMMA, PBA, and PBIS, respectively.[24]

We used dynamic light scattering (DLS) to measure the time correlation function of the scattered intensity $g^{(2)}(\tau)$ as a function of the decay time τ. The average hydrodynamic radius $\langle R_h \rangle$ and polydispersity of the samples were determined from analysis of $g^{(2)}(\tau)$ using either CONTIN[25] or cumulant analysis.[26] Z-average particle size distributions $f(R_h)$ were determined from CONTIN analysis.

The solid density of the particles was calculated from results of both static and dynamic light scattering measurements. The relatively narrow particle size distributions and the spherical shape of the particles allowed us to calculate the solid density ρ from the simple equation $M_w = (4/3)\pi\rho\langle R_h\rangle^3 N_A$.

Latex Thin Films. Latex films were made from aqueous dispersions of particles. The particle dispersions were either concentrated to ∼10 wt % and cast onto glass microscope slides or poured directly into glass dishes with flat bottoms. Sufficient dispersion was used to form a membrane with a thickness of ∼200 μm. The dispersions were partially dried at room temperature on a leveled plate. Before crack formation, they were incubated in an oven at 100−110 °C for 2−3 h. After incubation, the dry films formed in this way are generally flexible and robust. However, the mechanical strength of the films was found to drop on hydration. Some films were not sufficiently robust to be fully characterized.

Ionomeric Thin Films. 4.32 mL of MMA, 4.32 mL of BA, and either 1.05 or 4.32 mL of styrene were copolymerized using the same reaction conditions as used for precursor latex particle syntheses. The polymer was precipitated from methanol. Dried polymer was dissolved in chloroform and sulfonated by reaction with concentrated sulfuric acid at 50 °C for 0.5−3 h to obtain different degrees of sulfonation.[27] The resulting ionomer was dissolved in tetrahydrofuran (THF) before casting into thin films on Teflon plates. The final thickness of ionomeric thin films was ∼80 μm.

Gelatinous Thin Films. 400 mg of BIS and NaSS (0.203−1.03 g) were dissolved in a mixture of dimethylformamide (DMF, 8.0 mL) and water (1.3 mL). 2.16 mL of MMA, 2.16 mL of BA, 200 μL of N,N,N,N-tetramethylethylenediamine (TEMED), and 20 mg of KPS dissolved in 0.5 mL of water were added consecutively and mixed under a nitrogen atmosphere. A fraction of the pregel solution was transferred to a Petri dish containing a stack of several cover slides separated by 250 μm spacers while the rest of the solution (∼3 mL) was left inside the sealed vial so that the gelation process could be monitored. To remove oxygen, the dish was moved into a desiccator and alternately evacuated and exposed to nitrogen

10 times and then put aside in a sealed nitrogen atmosphere (∼1 atm) for 3 days for gelation and aging. The gel thin films were washed with acetone for ∼4 h to dissolve unreacted monomer.

Ion Exchange. Dried films were immersed in 2 M HCl to exchange Na^+ for H^+. After 24 h, the samples were washed with deionized water for more than 2 h before measurements of conductivity, *IEC*, and water uptake.

Film Characterization. The protonated membranes were pat-dried, and their masses and thicknesses were measured. The ion exchange capacity (*IEC*) of each film was measured by titration. Three samples of each membrane were individually immersed in approximately 15 mL of 2.0 M NaCl solution for at least 2 h. Solutions were titrated with 0.025 M NaOH to a phenolphthalein end point. After titration, the samples were rinsed with distilled water and dried under vacuum at 80 °C to constant mass. The *IEC* was calculated from the volume V_{NaOH} (mL) and concentration c_{NaOH} (mmol/mL) of NaOH and the dry mass m (g) of the film

$$IEC = \frac{V_{NaOH}c_{NaOH}}{m} \tag{2}$$

The water uptake was calculated as the ratio of the difference between the wet and dry masses of the film to the dry mass.

Proton Conductivity. The ac impedance spectra were measured in the frequency range 100 Hz−40 MHz using a gold-plated coaxial probe attached to a Hewlett-Packard 8753A network analyzer as previously described.[28] This geometry measures in-plane ionic conductivity.

TEM Characterization. Copper grids with carbon films, both Formvar and Formvar-free (Ted Pella Inc.), were used for TEM imaging. Dilute particle dispersions were cast onto the grids to form films ∼100 nm thick. All films were dried at room temperature unless specified. Films cast from ionomer solution were stained in saturated lead acetate for 48 h, washed and dried, embedded in epoxy resin cured at 60 °C overnight, and sectioned into ∼80 nm thick films. Unstained gel films were embedded in glycol meth-acrylate resin (Canemco Supplies) cured at 60 °C. TEM images were obtained using a Tecnai 20 scanning transmission electron microscope (FEI) at either 80 or 200 kV.

Neutron Scattering. Measurements were made at the Cold Neutron Research Facility at the National Institute of Standards and Technology (NIST) on the 30 m NIST-Exxon-University of Minnesota SANS instrument. A range of scattering wavevectors q from 0.003 to 0.1 Å^{-1} was obtained using three different configurations involving different sample to detector distances D_{s-d} and wavelengths λ: (i) $D_{s-d} = 1$ m and $\lambda = 6$ Å, (ii) $D_{s-d} = 7$ m and $\lambda = 6$ Å, and (iii) $D_{s-d} = 15.3$ m and $\lambda = 8.09$ Å. The samples were enclosed between two quartz windows separated by a gap of 1 mm; the space around the films was filled with D_2O, and the sample cells were maintained at ambient temperature during measurement.

Results and Discussion

Particle Synthesis. To obtain latex particles capable of forming a thin film with suitable mechanical strength, a variety of neutral monomers including styrene, *N*-isopropylacrylamide, acrylonitrile, butyl methyl acrylate, MMA, and BA were copolymerized with NaSS in latex particle synthesis. The combination of equal amounts of MMA and BA as the core components led to robust films that did not swell excessively and was found to be a good choice for the formation of ionic latex films.

Neutral Latex Particles. Figure 1a shows particle size information for neutral MMA−BIS−BA latex particles obtained from dynamic and static laser light scattering from particles dispersed in water at a concentration of 10^{-5} g/mL. The main graph shows the hydrodynamic radius distribution $f(R_h)$ obtained by CONTIN analysis of the dynamic light scattering data, and the inset shows a Zimm plot of static light scattering data. The

(a)

(b)
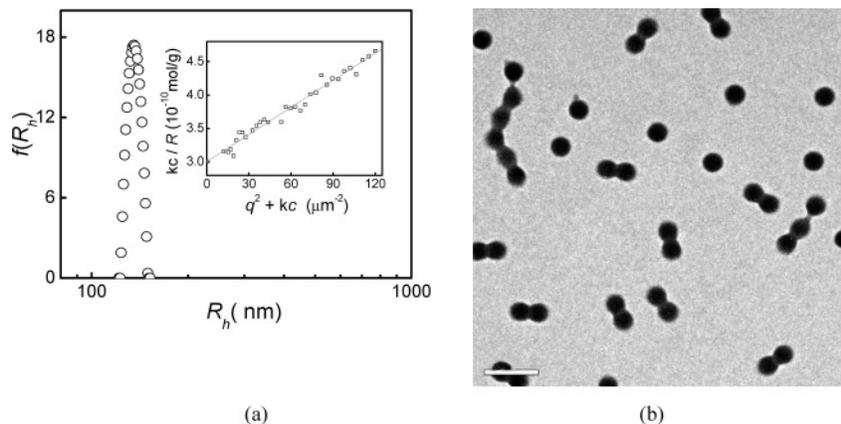
Figure 1. (a) Laser light scattering and (b) TEM characterization of MMA−BA−BIS neutral latex spheres reveal an average hydrodynamic radius of 135 nm in water and a radius of 90 nm in the dry state. The inset in (a) is a Zimm plot of data from static light scattering from which an average molar mass of 3.4×10^9 g/mol and a solid density of 0.53 g/cm³ are estimated. The bar in (b) represents 500 nm.

neutral particles were found to be very narrowly distributed with an average hydrodynamic radius $\langle R_h \rangle$ of 135 nm. By extrapolating the scattered intensity to $q = 0$, a molar mass $M_w = 3.4 \times 10^9$ g/mol and a solid density $\rho = 0.53$ g/cm³ were obtained. A TEM image of the particles, shown in Figure 1b, confirms that the particles are uniform spheres with a radius of 90 ± 0.5 nm in the dry state, consistent with the $\langle R_h \rangle$ and ρ values for swollen particles in water, assuming a density of 1.0 for dry spheres. Another important feature of the particles, which is essential for the formation of latex membranes, is the tendency for cohesion as a result of intersphere entanglement of the polymer molecules upon drying, evident from the distortion of contiguous spheres, as can be seen in Figure 1b.

Effect of Varying Total Monomer Concentration. The influence of total monomer concentration used in the synthesis on the properties of the resultant latex particles and their membranes was investigated in order to find a concentration range in which to investigate the synthesis of latex spheres containing different amounts of charge. Several batches of particles at a fixed mass ratio of MMA:BA:NaSS:BIS of (5.1): (4.9):(1.43):1, an initial *IEC* of the particles of 0.56 mmol/g, and a total monomer concentration ranging from 1.25 to 9.5 wt % of the total solution were synthesized. Figure 2 shows the size and solid density of the particles, measured in dilute dispersion where the particles are in a fully swollen state, and the final *IEC* and conductivity of the films made from them. The size increases and the density of the particles decreases as the initial monomer concentration is increased, while trends in the final *IEC* and conductivity of the films do not vary as significantly. At low monomer concentration, the conductivity is lower than average. There is an increase in both the final *IEC* and the conductivity of the batch made with the highest total monomer concentration indicating more efficient incorporation of charge.

Effect of Varying Initial Charge Content. The charge content of the particles was adjusted by varying the concentration of NaSS monomer in the reaction bath. The mass ratio of MMA, BA, and BIS was fixed at (5.1):(4.9):1 with the total concentration of neutral monomers fixed at 2.5 wt %. The concentration of NaSS was varied to achieve an *IEC* in the polymerization mixture ranging from 0 to 1.2 mmol/g. Figure 3 shows results for $\langle R_h \rangle$ and ρ for the resultant particles as measured in dilute solutions and the final *IEC* of the films produced from them. As the amount of NaSS in the reaction bath is increased, $\langle R_h \rangle$ and ρ decrease while an increase is observed in the final *IEC*. The three solid symbols represent
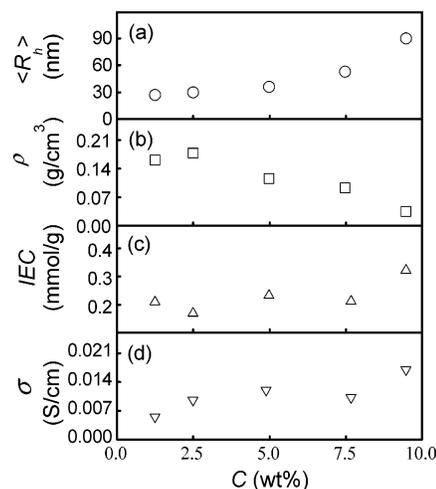
Figure 2. (a) Average hydrodynamic radius (circles), (b) average solid density of the precursor particles (squares) in dilute water dispersion, (c) final *IEC* (triangles), and (d) conductivity (inverse triangles) of thin films made from these particles as functions of the total monomer concentration in solution during synthesis. For all the batches included, the volume ratio of MMA to BA is 1, the mass ratio of BIS to total masses of MMA and BA is 10%, and the initial *IEC* of monomers in the feedstock is 0.56 mmol/g.

data for a sample synthesized in 0.1 M NaCl solution; these data will be discussed later in this section.

The trends of $\langle R_h \rangle$, ρ, and *IEC* are consistent with an increase in the charge incorporated as the initial charge content in the synthesis increases. The abrupt decrease in size observed when charge is incorporated is due to the well-known surfactant effect; the charged monomer acts as a polymerizable surfactant and leads to a reduction in particle size.[29] The density of particles decreases as more charge is incorporated because of electrostatically induced swelling of the particles.

Properties of the Films. The conductivities of the films produced using these particles are shown in Figure 4. To quantify the effectiveness of these films and advantages of them over less ordered structures, the properties of the latex particle films were compared to those of two other groups of films— gel films and ionomeric films—having similar compositions. The figure shows the dependence of the conductivity on final *IEC* for latex particle films (circles), gel films (triangles), and ionomeric films (squares). The results for different latex particle films made from the same batch of particles were averaged, and the error bars in Figure 4 represent the standard deviation of the mean of these measurements. The solid circle represents
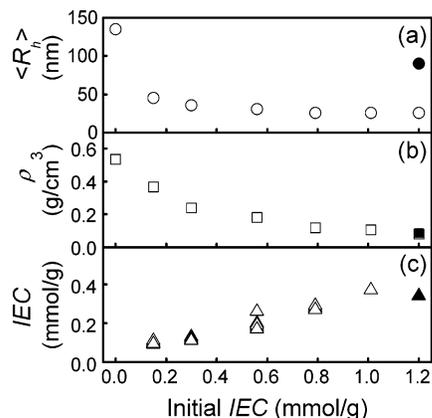
Figure 3. Dependence on initial charge content of (a) the average hydrodynamic radius (circles), (b) the average solid density (squares) of the precursor particles measured in dilute dispersions, and (c) the final *IEC* (triangles) of the thin films produced from them. The initial charge content is expressed as the initial *IEC* in mmol/g. For all of these batches, the volume ratio of MMA to BA is 1, the mass ratio of BIS to total mass of MMA and BA is 10%, and the total concentration of neutral monomers in the syntheses is 2.2 wt %. The three solid symbols to the right represent data for a sample synthesized in 0.1 M NaCl solution.
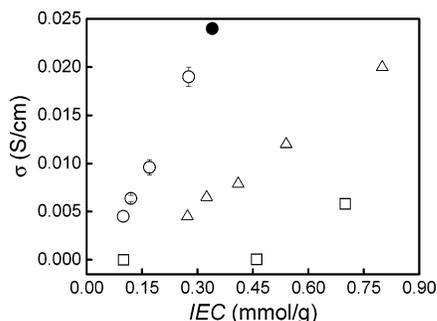
Figure 4. Relationship between the conductivity and the final *IEC* for the thin films prepared from poly(MMA−BIS−BA−NaSS) particles (circles), poly(MMA−BIS−BA−NaSS) gels (triangles), and sulfonated poly(MMA−BA−St) polymers (squares).

the conductivity of the thin film made from particles synthesized in 0.1 M NaCl.

The effect of structural design on final conductivity is clear from this graph. The latex films have conductivities significantly higher than those for both polymer gel films and films cast from ionomer solutions. The conductivity of the particle films is also higher than that measured in PS-*g*-macPSSA polymer membranes with similar charge content, which are known to form a network of ion channels.[28] This implies that, even though these other systems can achieve higher charge contents, the charges are less efficiently organized for proton conduction.

There are interesting differences in the relationships between conductivity and *IEC* for the three classes of material. The conductivity of the films cast from ionomer chains is negligible at low *IEC* and does not increase until the *IEC* is above ∼0.6 mmol/g. This relationship is similar to what is observed in many other types of ionomer membranes[30] and which has been described by percolation models.[31] On the other hand, both the latex films and the gel films are characterized by a linear relationship between conductivity and *IEC* with significant conductivity even at low *IEC*. This suggests that the percolation threshold either disappears or shifts to very low *IEC* values for membranes with bicontinuous structures.

The water content of proton-conducting polymers is an important property because transport phenomena, such as proton transport, oxygen permeability, and methanol crossover, are all associated with this characteristic. The average water uptake, as expressed as a wt % compared to the dried films, the average molar ratio of water absorbed per −SO_3H group, or λ value, and the average proton concentration for films made of latex particles, gels, and ionomer chains are shown in Figure 5 as functions of the final *IEC*. For all membranes, the water uptake increases as the charge content increases. Membranes made from particles synthesized in water with final charge contents above 0.4 mmol/g swell excessively and are too soft for further measurements. Gel membranes with high *IEC*s also swell excessively as seen by a very high water uptake of 1200 wt % and λ value of 830 for gel membranes with an *IEC* = 0.8 mmol/g. Above *IEC*s of 0.8 mmol/g, gel membranes lose mechanical strength, and no further measurements are possible. In general, λ values are high, indicating that the protons are moving in an environment that looks like bulk water.[32] Below *IEC*s of 0.4 mmol/g, the water uptake, λ values, and proton concentration are similar in samples of comparable *IEC* for all three systems, while the conductivity varies by orders of magnitude between samples. This indicates that the water content alone cannot account for differences in proton conductivity observed in these three systems and suggests that the range of conductivities observed is related to the organization of charge within the membranes, which varies with the structure of the films.

Effect of the Presence of Salt on Particle Synthesis. In an attempt to increase the charge content of the particles, we synthesized one batch of particles in 0.1 M NaCl. We hypothesized that the ions in solution would screen the charge on the surface of the particles and result in tighter packing of charge and higher conductivity. Data for these particles and films made from them are shown using solid symbols in Figures 3−5. As recorded in Figure 3, the size of the particles synthesized in NaCl is more than 3 times larger than that of particles synthesized from the same components in the absence of salt. This is consistent with other studies of particle formation in the presence of salt, where addition of a salt or a charged surfactant leads to the formation of larger particles because of screening of the surface charge of the growing particles.[33] The solid density of the particles, on the other hand, is the same. The salt was removed from the particle dispersion by dialysis before film formation because crystallization of salt in the dispersion as the water evaporates can cause cracking of latex films. The final *IEC* of the thin film made from the dialyzed particles is slightly lower than the trend observed for the other particles. This may be due to the fact that these dispersions were dialyzed and the others were not. It is possible that linear chains with higher charge content coexist with the particles; we have not been able to separate or quantify these. Loss of these chains during dialysis would result in these films having a lower final *IEC*. Even so, films made from these particles had higher conductivity than any other particle film as shown by the solid circle in Figure 4, presumably because the charges are more tightly packed on the surface of the particles. Note that films made from particles synthesized in pure water at this charge concentration were too soft to measure. The conductivity of films made from these particles is consistent with the linear trend observed in the films made from particles synthesized in the absence of salt.

Charge Coverage Achieved. The fraction of the particle surface that is covered by charged groups can be estimated by comparing the measured *IEC* and the maximum attainable *IEC*_max. For a given charge content, the *IEC* depends on the number of charge groups per particle *n* and the number of
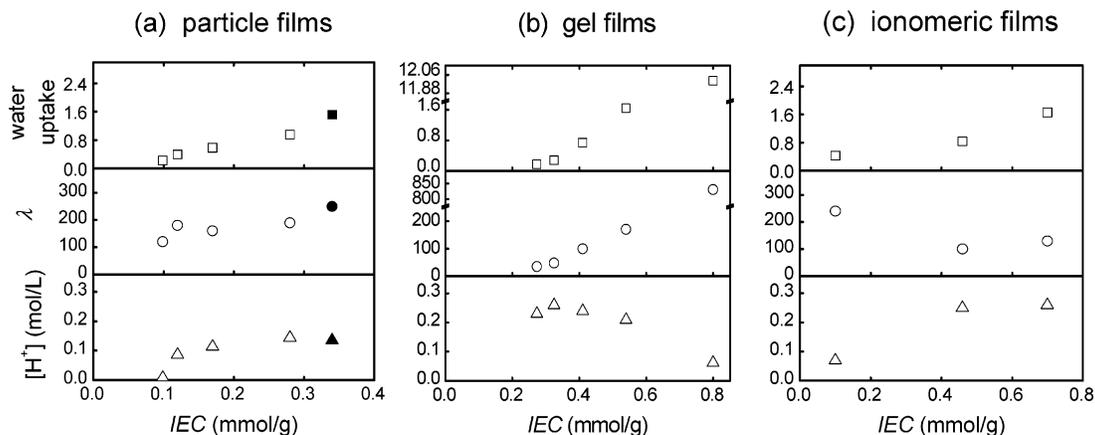
Figure 5. Water uptake (squares), λ values (circles), and proton concentration (triangles) for (a) latex, (b) gel, and (c) ionomeric thin films. The solid symbols represent data for the thin film made with particles synthesized in NaCl.
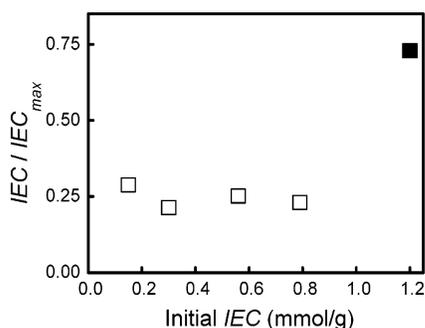
Figure 6. IEC of the final film as compared to the maximum possible value as a function of the initial charge content calculated using the characteristics of the particles in the final thin films. The solid symbol represents data for particles synthesized in 0.1 M NaCl.

particles produced per gram of solid material N:

$$IEC = \frac{nN}{N_A} \qquad (3)$$

If monolayer coverage is assumed, the maximum number of charged groups per particle is

$$n_{max} = \frac{A}{a_0} \qquad (4)$$

where A is the surface area of the particle $A = 4\pi R^2$ and a_0 is the cross-sectional area of the individual charged groups. Making the substitution $N = 1/m$, where m is the mass of each individual particle, IEC_{max} can be expressed in terms of a_0, N_A, the density ρ, and the radius of the particle R

$$IEC_{max} = \frac{3}{a_0 \rho R N_A} \qquad (5)$$

The average area of a charged group was estimated to be $a_0 = 0.5$ nm^2 from values of the size of the headgroups of standard surfactants.[34] Values for ρ and R for the swollen films were estimated using the density and size of the particles measured in dilute dispersions and the water uptake for the films. Results for the ratio IEC/IEC_{max}, or equivalently surface coverage, as a function of the initial charge content are shown in Figure 6. The surface coverage for the films made with particles synthesized in water is roughly 25% of the maximum that can be obtained, while films made with particles synthesized in NaCl achieve 75% of IEC_{max}, assuming monolayer coverage. These results indicate that we have not achieved full coverage of the

particles during synthesis but that this is improved when particles are synthesized in salt, probably because screening of the charge during synthesis enables tighter packing of the charged units on the surface of the particles.

Electron Microscopy. We used TEM to image the latex particles and the associated thin films in the dry state. Figure 7a shows an image of charged spheres made with an initial IEC of 0.15 mmol/g. These particles were deposited onto TEM grids from an aqueous dispersion. The samples were not stained. We believe that the contrast between the surface regions and the cores is confirmation that the charge groups are localized at the surface of the particles, as the electrons will be scattered more strongly from the charge groups leaving a darker image. Localization of the charge at the surface is expected for particles made in water.[29] When the same spheres are deposited from ethanol rather than water dispersions, the particles have a more grainy appearance, as seen in Figure 7b. We attribute the graininess to microphase separation of the charged groups on the surfaces. This should occur more readily in ethanol than water because ethanol is a poor solvent for NaSS. The phase separation is constrained because spheres consist of cross-linked polymer chain networks. Figure 7c is a TEM image of a latex film made from the batch of particles made in NaCl (initial IEC of 1.2 mmol/g) cast onto TEM sample grids and then incubated for 3 h at 102 °C. This image is characterized by an even grainier texture, but individual particles can still be discerned, confirming that particle structure remains even after incubation. Images of unstained gel films (Figure 7d) with IEC of 0.8 mmol/g show more uniformly distributed tiny black dots of ionic clusters together with some patches of denser regions, implying less efficient channels for proton conduction. Figure 7e is a typical image of an ionomeric film stained with lead acetate solution that shows amorphous structure consistent with its much lower conductivity. Figure 7f is an image of the same film taken 2 min later; this film is not stable to bombardment by the electron beam, and coarsening of the structure is observed. This provides supplemental evidence of low connectivity of the conduction path in these samples; if continuous pathways exist, electron energy is usually dissipated quickly enough to avoid damage.

Neutron Scattering. Neutron scattering spectra have been measured for several dispersions of particles and for films made from them. One advantage of these measurements as compared to TEM imaging is that they are made on hydrated samples. Results for particles made with an initial charge content 0.15 mmol/g and dispersed in D$_2$O are shown in Figure 8. Also shown are results for films made from these particles and
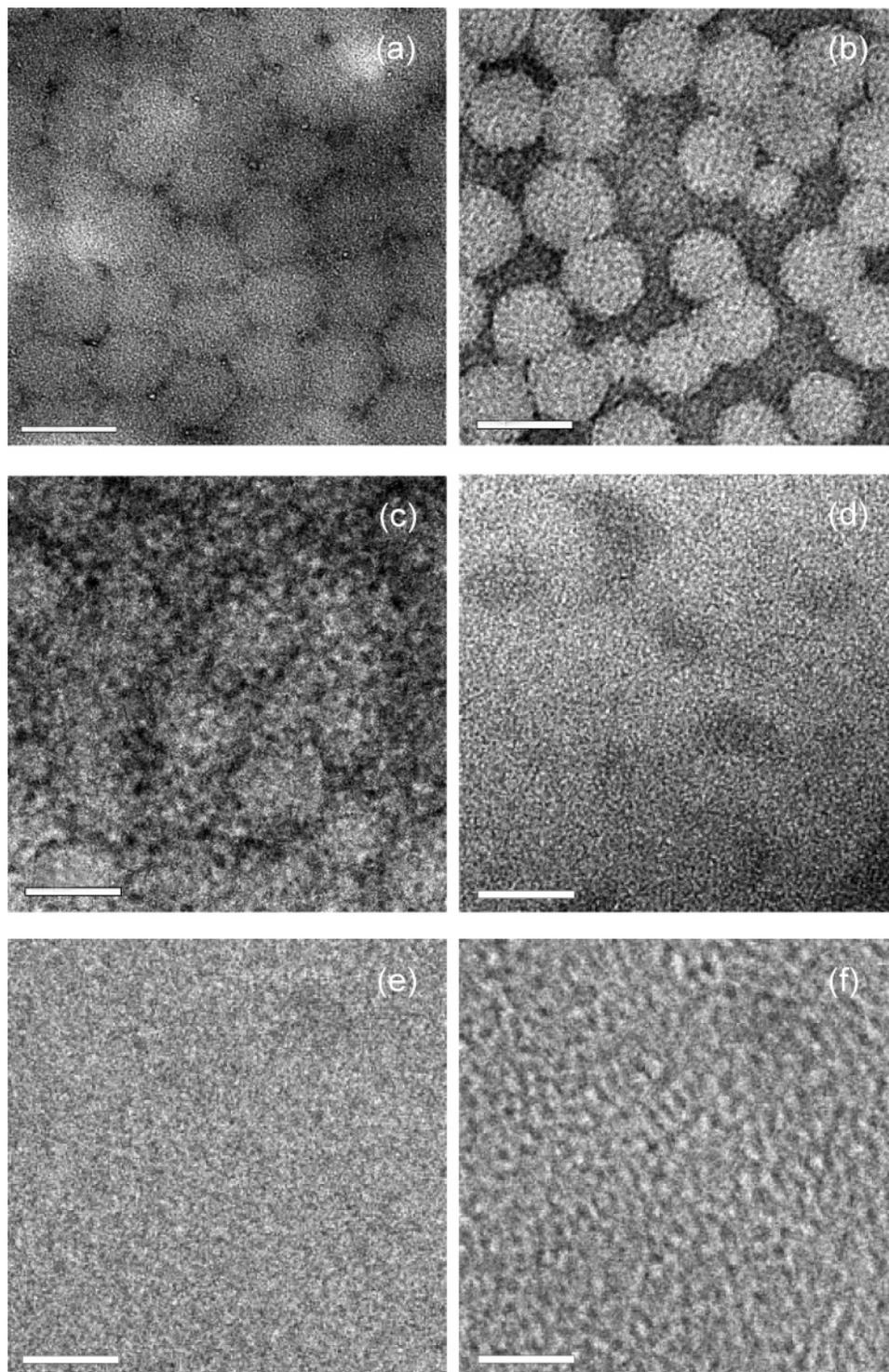
Figure 7. TEM images of (a) closely packed lightly charged particles (initial *IEC* of 0.15 mmol/g) cast at room temperature on a TEM grid from dilute water dispersion, (b) same particles cast from dilute ethanol dispersion, (c) a film cast from a dialyzed water dispersion of the particles synthesized in NaCl and incubated at 102 °C for 3 h, (d) an unstained gel film with *IEC* of 0.8 mmol/g, (e) a snapshot of the film cast from ionomer solution having an *IEC* of 0.7 mmol/g, and (f) the same region of the same film after exposure to the electron beam for less than 2 min. Images a−d were obtained at an accelerating potential of 200 kV while that for images e and f was 80 kV. All bars represent 100 nm.

swollen in D_2O. The scattering from the particles (open circles) shows a first minimum and evidence of a second, as is characteristic of polydisperse spheres in solution. A fit of the data using the form factor for polydisperse spheres indicates that the average radius of the spheres is 35 nm with a polydispersity of 15%. The scattering from the particle film clearly indicates that this structure persists. There is no evidence for smaller scale structure suggested by the graininess observed in the TEM images of similar particles and films. TEM images

are made in a vacuum while the neutron scattering spectra are from hydrated samples; it is possible that if the graininess observed by TEM is attributable to isolated charge clusters, these may form continuous hydrophilic channels upon hydration.

Conclusions

We have made charged latex particles by copolymerizing MMA, BA, and NaSS and have used these to make latex films. After exchanging the Na^+ with H^+, the latex membranes show
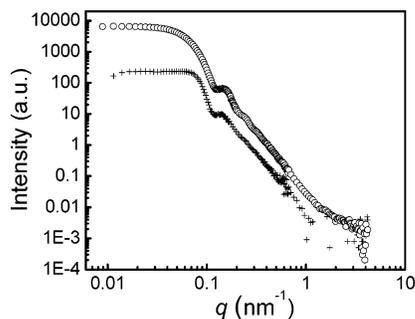
Figure 8. Neutron scattering measurements for particles (circles) and a film (crosses) made from particles with an initial charge content of 0.15 mmol/g. The film was incubated at 100 °C for 2 h. The interparticle distance is consistent with the particle size measured in dilute water dispersion.

significant proton conductivity. In fact, the membranes show much higher proton conductivity at low charge contents than films made of ionomer chains or polymer gels of similar compositions. Membranes made from both latex particles and polymer gels have conductivities that increase linearly with *IEC*, in contrast to most other systems where the conductivity is very low at low charge content, behavior typical of a percolation transition. Comparison of the three systems emphasizes the importance of controlling the structure of the conducting regions in order to achieve good proton conductivity. However, we have observed that incorporation of charge into latex membranes, and consequently their conductivity, appears to be limited by two factors: the amount of charge that can be incorporated into the particles,[29] and the excessive swelling of the membranes that occurs as they become more hydrophilic. TEM and neutron scattering confirm the particulate structure of these membranes.

References and Notes

(1) Hickner, M. A.; Ghassemi, H.; Kim, Y. S.; Einsla, B. R.; McGrath, J. E. *Chem. Rev.* **2004**, *104*, 4587.
(2) Savadogo, O. *J. Power Sources* **2004**, *127*, 135.
(3) Roziere, J.; Jones, D. J. *Annu. Rev. Mater. Res.* **2003**, *33*, 503.
(4) Li, Q.; He, R.; Jensen, J. O.; Bjerrum, N. J. *Chem. Mater.* **2003**, *15*, 4896.
(5) Kerres, J. A. *J. Membr. Sci.* **2001**, *185*, 3.
(6) Rikukawa, M.; Sanui, K. *Prog. Polym. Sci.* **2000**, *25*, 1463.
(7) Yang, Y.; Holdcroft, S. *Fuel Cells* **2005**, *5*, 171.
(8) Yeager, H. L. Transport Properties of Perfluorosulfonate Polymer Membranes. In Eisenberg, A., Yeager, H. L., Eds.; *Perfluorinated Ionomer Membranes*; ACS Symp. Ser. **1982**, *180*, 49.
(9) Yin, Y.; Fang, J.; Watari, T.; Tanaka, K.; Kita, H.; Okamoto, K. *J. Mater. Chem.* **2004**, *14*, 1062.
(10) Kim, H.-J.; Cho, S. Y.; An, S. J.; Eun, Y. C.; Kim J.-Y.; Yoon, H.-K.; Kweon, H.-J.; Yew, K.-H. *Macromol. Rapid Commun.* **2004**, *25*, 894.
(11) Gil, M.; Ji, X. L.; Li, X. F.; Na, H.; Hampsey, J. E.; Lu, Y. F. *J. Membr. Sci.* **2004**, *234*, 75.
(12) Karlsson, L. E.; Jannasch, P. *J. Membr. Sci.* **2004**, *230*, 61.
(13) Chen, N. P.; Hong, L. *Polymer* **2004**, *45*, 2403.
(14) Smitha, B.; Sridhar, S.; Khan, A. A. *Macromolecules* **2004**, *37*, 2233.
(15) Ponce, M. L.; de A. Prado, L. A. S.; Silva, V.; Nunes, S. P. *Desalination* **2004**, *162*, 383.
(16) Nakajima, H.; Honma, I. *Solid State Ionics* **2002**, *148*, 607.
(17) Yamaguchi, T.; Miyata, F.; Nakao, S. *Adv. Mater.* **2003**, *15*, 1198.
(18) Rubatat, L.; Rollet, A. L.; Gebel, G.; Diat, O. *Macromolecules* **2002**, *35*, 4050.
(19) Zaluski, C.; Xu, G. *Macromolecules* **1994**, *27*, 6750.
(20) Gao, J.; Lee, D.; Yang, Y. S.; Holdcroft, S.; Frisken, B. J. *Macromolecules* **2005**, *38*, 5854.
(21) Eckersley, S. T.; Rudin, A. Film Formation of Acrylic Copolymer Latices: A Model of Stage II Film Formation. In Provder, T., Winnik, M. A., Urban, M. W., Eds.; *Film Formation in Waterborne Coatings*; ACS Symp. Ser. **1996**, *648*, 2.
(22) Liu, R.; Winnik, M. A.; Stefano, F. O.; Vanketessan, J. *Macromolecules* **2001**, *34*, 7306.
(23) Zimm, B. H. *J. Chem. Phys.* **1948**, *16*, 1099.
(24) Brandrup, J., Immergut, E. H., Grulke, E. A., Eds.; *Polymer Handbook*; John Wiley & Sons: New York, 1999.
(25) Provencher, S. W. *Makromol. Chem.* **1979**, *180*, 201.
(26) Chu, B. *Laser Light Scattering*; Academic Press: Boston, 1991.
(27) Weiss, R. A.; Sen, A.; Willis, C. L.; Pottick, L. A. *Polymer* **1991**, *32*, 1867.
(28) Ding, J.; C. Chuy, S. Holdcroft, *Macromolecules* **2002**, *35*, 1348.
(29) Kim, J. H.; Chainey, M.; El-Aasser, M. S.; Vanderhoff, J. W. *J. Polym. Sci., Part A: Polym. Chem.* **1992**, *30*, 171.
(30) Shi, Z. Q.; Holdcroft, S. *Macromolecules* **2005**, *38*, 4193.
(31) Hsu, W. Y.; Barkley, J. R.; Meakin, P. *Macromolecules* **1980**, *13*, 198.
(32) Krueuer, K. D. *J. Membr. Sci.* **2001**, *185*, 29.
(33) Peach, S. *Macromolecules* **1998**, *31*, 3372.
(34) Stubbs, J. M.; Durant, Y. G.; Sundberg, D. C. *Langmuir* **1999**, *15*, 3250.